Granular Matter
DOI 10.1007/s10035-013-0420-1

ORIGINAL PAPER

Evolution of ultrasonic velocity and dynamic elastic moduli with shear strain in granular layers

Matthew W. Knuth · Harold J. Tobin · Chris Marone

Received: 14 December 2012

Abstract Ultrasonic wave transmission has been used to investigate processes that influence frictional strength, strain localization, fabric development, porosity evolution, and friction constitutive properties in granular materials under a wide range of conditions. We present results from a novel technique using ultrasonic wave propagation to observe the evolution of elastic properties during shear in laboratory experiments conducted at stresses applicable to tectonic faults in Earth's crust. Elastic properties were measured continuously during loading, compaction, and subsequent shear using piezoelectric transducers fixed within shear forcing blocks in the double-direct-shear configuration. We report high-fidelity measurements of elastic wave properties for normal stresses up to 20 MPa and shear strains up to 500 % in layers of granular quartz, smectite clay, and a quartz-clay mixture. Layers were 0.1–1 cm thick and had nominal contact area of 5cm × 5cm. We investigate relationships among frictional strength, granular layer thickness, and ultrasonic wave velocity and amplitude as a function of shear strain and normal stress. For layers of granular quartz, P-wave velocity and amplitude decrease by 20–70 % after a shear strain of 0.5. We find that P-wave velocity increases upon application of shear load for layers of pure clay and for the quartz-clay mixture. The P-wave amplitude of pure clay and quart-clay mixtures first decreases by ∼50 and 30 %, respectively, and then increases with additional shear strain. Changes in P-wave speed and wave amplitude result from changes in grain contact stiffness, crack density and disruption of granular force chains. Our data indicate that sample dilation and shear localization influence acoustic velocity and amplitude during granular shear.

Keywords Wave speed · Friction · Shear strain · Ultrasonic properties

1 Introduction

The behavior of seismogenic crustal faults remains a major problem in geophysics (e.g. [54]), and recent large earthquakes and tsunamis serve as a reminder of the societal and scientific importance of improving our understanding of granular materials within earthquake fault zones. Great earthquakes often extend for 100's of kilometers, however the physical processes that dictate earthquake nucleation and rupture propagation are largely controlled by micromechanics occurring at the fault interface (e.g. [86–90]). Because these processes are largely inaccessible from Earth's surface, remote sensing techniques such as seismic wave propagation are important for investigating the basic mechanical behavior of tectonic faults [30,45,50,64,97,101,110,111]. Laboratory experiments on granular and clay-rich fault zones play an important role in identifying the fundamental processes and relevant scales of faulting [2,13,14,19,20,24,29,31,39,48,49,61,62,70,80,95].

The strength and failure mechanics of cataclastic faults are controlled by properties of the surrounding wall rock and the mechanical behavior of fault gouge (e.g. [9,12,17,20,22,26,42,65,79,87–89,96,103]). Laboratory experiments on granular mechanics can play a key role in linking field observations to theory and numerical models of

M. W. Knuth · H. J. Tobin
Department of Geoscience, University of Wisconsin-Madison, 1215 W Dayton St., Madison, WI 53706, USA

C. Marone (✉)
Department of Geosciences, The Pennsylvania State University, University Park, PA 16802, USA
e-mail: cjm38@psu.edu

Published online: 10 May 2013

the underlying physics [8,24,30,32,40,66,105–107]. Moreover, by combining measurements of ultrasonic properties with friction and deformation properties (e.g., [49]), one can illuminate deformation mechanisms in granular materials that are not detected by conventional studies of friction [4,45,75,90,100,102].

The purpose of this paper is to introduce a novel technique for measurement of elastic properties during high strain tests at elevated pressure and to present new results for the evolution of elastic moduli with shear under geophysical stresses. We apply the technique to granular and clay-rich materials, which simulate the wear materials (gouge) found in tectonic fault zones. We focus in particular on the connections between frictional and elastic properties, and their evolution as a function of shear strain. We find that the evolution of ultrasonic properties with shear varies significantly from granular to clay rich samples. We show that continuous ultrasonic monitoring during laboratory deformation adds new insight to physical processes and transient physical properties of sheared granular materials, and is an important tool for experimental investigation of friction in rocks and granular materials.

1.1 Background

The basic mechanical parameters that describe granular and porous geological material include both intragranular, intergranular, and geometric effects [6,11,16,34,44,51,84]. These include the stiffness and density of the grains themselves (e.g. [7,56,59,100]) and the particle contacts described by Hertz-Mindlin contact theory and modulated by cementation and pore-fluid interactions (e.g. [4,9,21,33,38,48,49,63,70]). The relative contributions of these processes are determined in part by interactions within the network of grain-grain contacts and the stresses at individual contacts (e.g. [15,34,44,45,62,63,93,94,98]). Interactions between the granular framework and pore fluid pressure are described by Biot theory and poroelasticity (e.g. [18,25,28,35,68,91,92,101,104,108]).

Mechanical energy travels through granular media via elastic transmission between particles, and thus the elastic properties of granular layers depends on the ambient stress field in the region(s) they pass through (e.g. [3,5,44,57,64]). The application of quasi-static loads cause deformation described by the quasi-static elastic moduli of a material, whereas dynamic, short-term stresses (e.g., ultrasonic waves) sense a range of dynamic moduli (e.g [1,108]).

A stress exerted on the boundary of a granular system will be divided among weak interparticle contacts and localized "force chains" carrying substantially higher loads and supporting the sample (e.g., [77,81]). The stiffness of single grains in a granular pack may be less important to bulk elastic wave speed than the effective stiffness of the framework.

Empirical relationships between stress and strain are commonly used to infer static elastic parameters of geomaterials (e.g. [10]). However, the strains required to derive static elastic moduli in this manner may be large and disruptive, and the experimental configurations used often prohibit simultaneous measurement of friction constitutive parameters and shear fabric (e.g., [36,65]). Ultrasonic velocity measurements can be used to derive elastic properties and have the advantage that induced changes in stress are small and produce negligible permanent deformation (e.g. [49,82]). Ultrasonic wave properties are a function of the bulk and shear moduli of the material they traverse. Thus dynamic elastic moduli may be obtained without disturbing the in-situ, and sometimes fragile network of particle contacts that form during compaction or shearing. Because granular materials are inherently dispersive, their dynamic elastic properties vary as a function of ultrasonic probing frequency and under dynamic stressing (e.g. [49,63,72,73,83,85,91]). Moreover, when subject to shear, granular media are often in a state of fragile, unrecoverable failure; thus, a simple stress vs. strain curve during frictional sliding does not provide a true measurement of the quasistatic moduli. However, because the deformation associated with the passage of ultrasonic waves is recoverable, wavespeed measures can be used to derive elastic moduli continuously as a function of deformation and failure [49].

In geophysics, sonic borehole logging has driven a great deal of research into how wavespeed changes during compaction of sediments (e.g., [3,37,97]). A common goal in such studies is to produce velocity models from active-source seismic imaging. Such models require calibration between pressure, porosity, and ultrasonic velocity [110,112]. Despite the interest in compaction behavior, comparatively little work has been done on the evolution of granular materials subjected to shear strain.

2 Methods

2.1 Double direct shear

The biaxial double-direct-shear configuration is designed to measure the frictional and mechanical properties of granular materials including simulated fault gouge (Fig. 1). This configuration consists of two layers of sample material sandwiched between three rigid forcing blocks (e.g. [27]). Shear is forced to occur within the granular material by strong coupling at the bounding surfaces produced by grooves oriented perpendicular to the shearing direction. (e.g. [19,20,42,53,61,87]). In this study, forcing blocks were constructed from tool steel and the nominal frictional contact was 5 cm $\times$ 5 cm.

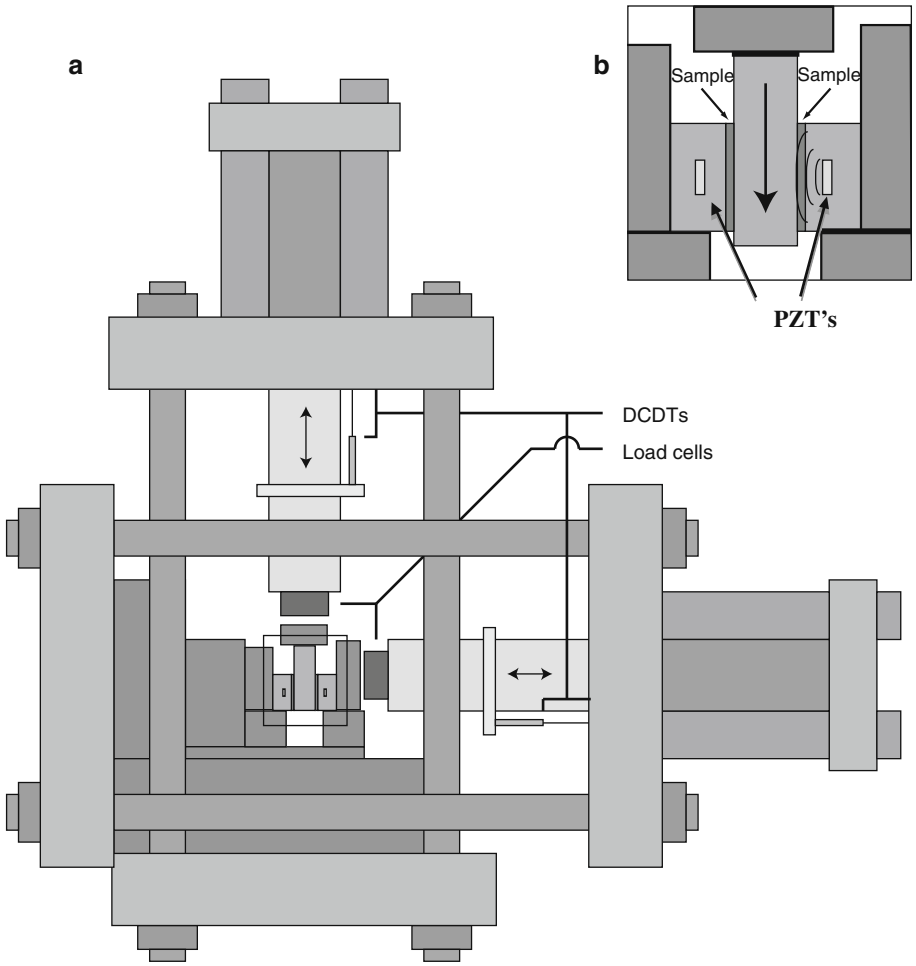

Fig. 1 **a** The biaxial deformation apparatus used for our experiments. Normal stress on the frictional surfaces is applied by the horizontal ram. Shear is driven by the vertical loading ram. **b** Detail of the double direct shear assembly showing embedded piezoelectric transducers (PZT), which transit P and S-waves. Frictional contact area is 50 mm × 50 mm

We studied granular layers composed of quartz, a smectite clay, and mixtures of the two (Fig. 2). Shear and normal stresses are calculated from applied forces and the dimensions of the sample. Shear and volumetric strains are calculated from shear displacement and normal displacement of the layer boundaries. All displacement and strain measurements are reported for a single layer, assuming symmetric behavior for the double direct shear configuration (Fig. 1). Stresses are derived from measurement of force made with strain gauge load cells accurate to ±10 N (0.4 KPa on our layers). Displacements at the layer boundaries are measured with DCDT's accurate to ±0.1 μm. Displacements are corrected for elastic distortion of the loading frame. Together, these data are used to derive stresses and frictional properties of the sample under a wide range of conditions. In total, 26 experiments were conducted for this study.

2.2 Ultrasonic velocity measurements

Ultrasonic transmission waveforms were recorded continuously during shear experiments using a direct transmission technique with piezoelectric crystal sources. The acoustic sources and receivers were 0.5-inch diameter cylindrical lead-zirconate-titanate (PZT) crystals with vacuum-deposited, chrome-gold electrode surfaces and a center frequency of 0.5 MHz. We embedded the transducers in the side blocks of the double-direct shear assembly using a silver-filled conductive epoxy (Fig. 1). The PZT's were 7 mm from the base of the grooves in the side blocks. P and S-wave arrivals were identified in the recorded waveforms based on one-way time-of-flight through both layers in the double-direct shear configuration (Fig. 1), after correcting for travel-time within the steel blocks as determined by calibration.

We used an Olympus NDT Model 5058PR pulser-receiver to apply 900-volt pulses (0.1–4 μs pulse width) to the source transducer at a repetition rate of 100 Hz. The output from the receiver transducer was recorded by a GaGe CS8382 multi-channel digitizer at a rate of 25 MHz at 14-bit depth over a 1 or 2-volt range. One hundred waveforms were stacked for each output measurement followed by a 1 s pause to transfer data and reset the acquisition card, for an effective recording rate of full waveforms of 0.5 Hz.

The relative amplitude of individual waveforms varies as a function of attenuation and efficiency of the source

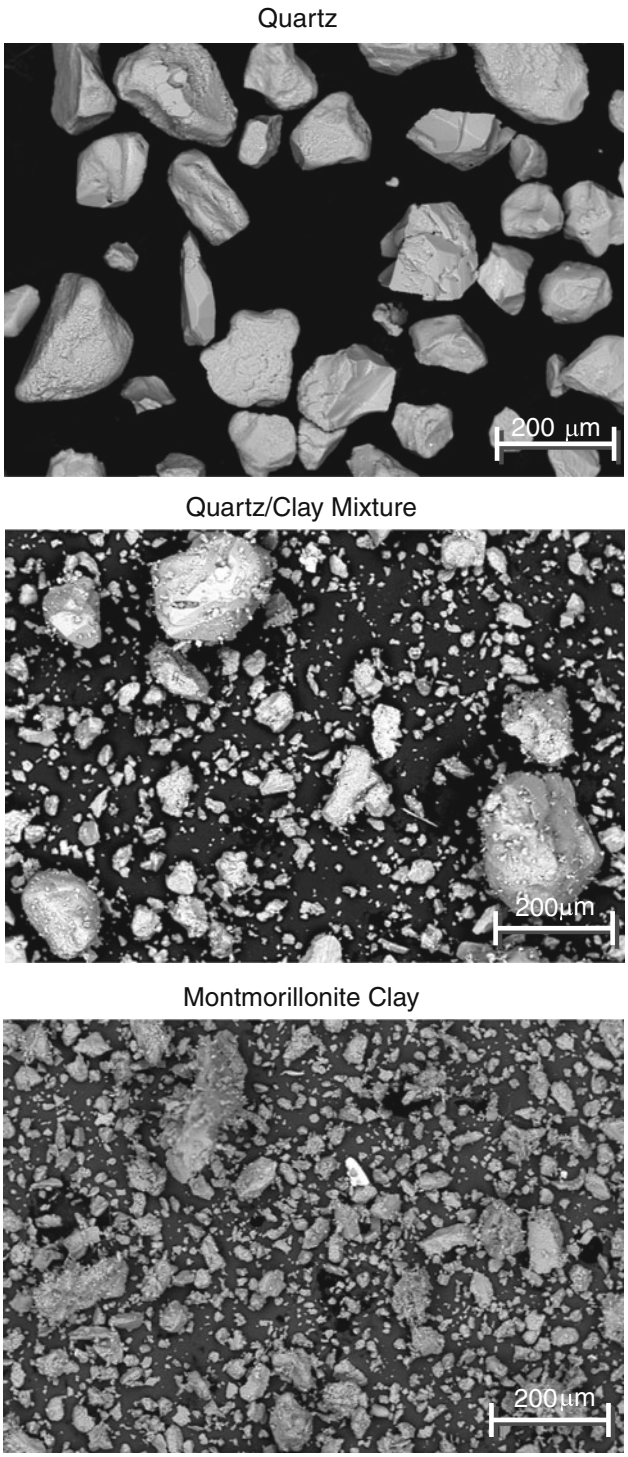

Fig. 2 SEM images of the sample materials, showing the starting materials for each of the three sample types used

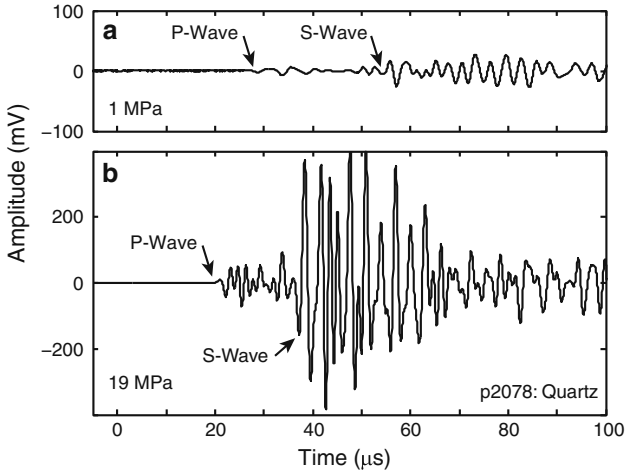

Fig. 3 Example ultrasonic waveforms indicating P and S-wave arrivals from experiment p2708 on a granular quartz layer at **a** 1 MPa applied normal stress and **b** 19 MPa applied normal stress. Note the distinct P and S wave arrival and the large increase in amplitude caused by increased normal stress

transducers. The difficulty of comparing absolute wave amplitude between experiments using acoustics is well known and arises from differences in coupling, transducer response, and path length of the transmitted wave. Our approach circumvents much of this problem because we have a fixed set of transducers and are able to record waveforms continuously as a function of applied stress and strain evolution for complex loading histories. In addition to tracking changes in a given experiment, we compared ultrasonic waveforms between experiments by working with relative wave amplitudes rather than absolute amplitude corrected for attenuation [52].

For our configuration, many of the factors that relate attenuation and amplitude are constant within a given experiment. Thus changes in amplitude as a function of shear and other factors can be used to infer changes in internal properties such as porosity, particle size distribution, and fabric development [16,48,76]. The amplitude of the P and S-wave arrivals varied from millivolts to hundreds of millivolts within the same experiment depending on strain and applied normal stress (Fig. 3).

2.3 Sample preparation

We studied granular, clay and mixed composition layers. (Fig. 2). Our suite of samples was selected to include the end-member compositions expected for gouge found in tectonic fault zones, and also to connect with a large body of existing literature on frictional and mechanical properties of simulated fault gouge (e.g., [2,12,19,20,24,42,53,55,60,78,80]).

The granular quartz was a high-purity (>99 % quartz), fine-grained material purchased from the U.S. Silica company as F110 foundry sand; 95 % of the grains are in the range 53–212 μm and the mean grain size is 127 μm. F110 is a common laboratory standard for granular studies, and its frictional properties are well established over a wide range of conditions (e.g. [2,60,66]). The clay is calcium mont-

morillonite purchased as a dried powder (GSA resources, SM1502A). XRD analysis shows that this material is 90 % clay, 2 % quartz, and 8 % plagioclase, and that the clay-sized fraction is 100 % smectite (M. Underwood, pers. comm.). The grain size of this material is polydisperse, with individual crystallites forming clumps over a size range from ~10 to 200 μm and peaking at ~75 μm as measured in a Mastersizer particle size analyzer. In addition to the end-members, we studied a 50/50 mixture, by mass, of the quartz and clay.

Sample layers were constructed by forming a cellophane tape wall around the perimeter of a 5 cm × 5 cm side-block and filling to a predetermined height (e.g., [53]). For initial handling, the sample blocks were secured together with strips of tape. These were removed after samples were loaded into the testing machine. To prevent material loss during shearing, thin copper shims were fixed to the underside of the blocks and further secured by a thin elastic membrane. Guide plates were bolted to the outside (front and back) of the side blocks to prevent extrusion of the sample in the out-of-plane direction (Fig. 1).

2.4 Wave speed and arrival-time picking

The path length between the PZT's in the shear configuration is on order of only a few centimeters (Fig. 1). Thus, P-wave arrivals had to be identified precisely and consistently. For example, at a digitizing rate of 25 MHz with a pair of 5-mm thick layers and P-wave velocity of 2,000 m/s, the effective resolution is 20–30 m/s. This resolution in velocity decreases as the path length decreases, reaching ±50 m/s for a pair of 1.5-mm sample layers. Waveforms are acquired as the response of a 500 KHz transducer, so any high-frequency "spike" arrival will appear as the first oscillation in a waveform with a dominant period of 2 microseconds. The arrival time of the wave is indicated by the first point in time where the oscillation emerges from the background noise. Because of dispersion and attenuation [52] both the shape and the amplitude of a band-limited waveform will evolve with changes in ultrasonic velocity, path length, or other factors that influence attenuation [71,72,97,111].

A traditional method is to pick phase arrivals by visual inspection using the emergence of a waveform above background noise. Another approach is to use the first minimum or maximum [50]. A more precise method is to estimate the arrival time for a single waveform manually, and then calculate the offset in time between that and other waveforms through cross-correlation (e.g. [71,74]). This technique is sensitive to changes in the shape of the waveform, and will produce false positives in band-limited waveforms where the first arrival comes in at significantly lower amplitude than subsequent sections of the wave.

Because the noise in the waveform prior to the P-wave arrival was quite small in our measurements, we applied a simple, automated edge-finding procedure to identify the boundary between the portion of the waveform with coherent amplitude and that without. For each point k in waveform X, this algorithm takes the absolute value of two windows of length n.

$$D_k = \sum_{i=k}^{k+n} abs(X_i) \Big/ \sum_{i=k-n}^{k} abs(X_i)$$

Maxima in D indicate where a sum of large values is being divided by a sum of near-zero values, which occurs at the P-wave arrival when low-frequency noise is absent prior to the onset of the compressional wave.

We also tested a simple Akaike Information Criterion-based (AIC) method after the formulation of [58] as reported by [106]. This compares the variance before and after each point k in waveform X of length n.

$$AIC_k = k \cdot \log\{\mathrm{var}(X[1,k])\} + (n-k-1) \cdot \log\{\mathrm{var}(X[k+1,n])\}$$

The AIC technique is essentially a measure of "goodness-of-fit" between a signal and a model. The AIC coefficient is lowest where the waveform changes in overall character, reaching local minima at the EM wave and the P-wave arrival. The results for our waveforms were comparable with the edge-finding algorithm. The AIC technique performs better in cases with low signal to noise ratio prior to the P-wave arrival and/or where noise has significantly different frequency content and variance compared to the P-wave.

Our initial experimental configuration was instrumented with a single P-wave transducer on either side of the sample (Fig. 1). We also used shear-cut crystals in an orientation that produces a high-amplitude S-wave with a particle motion parallel to the shearing direction of the sample layers. These also produce a distinct P-wave via mode conversion at the interface of the layer and forcing block. Despite their lower amplitude expression, compressional waves generally obscure the arrival of the shear wave in recorded data. Although the P-waves can be picked from the emergence of a coherent signal above the background noise, S-waves must be picked as time- or displacement-variant changes in the shape of the waveform followed by a significant increase in amplitude. This is difficult to automate with algorithms used to detect P-wave arrivals, so S-wave arrivals were picked manually on a subset of waveforms and interpolated using a minimum-curvature spline fit between picks.

We determined ultrasonic velocity by measuring changes in arrival time and path length. For experiments where both P-wave and S-wave arrivals were measured, we calculated elastic moduli using the relationships

$$V_P = \sqrt{\frac{K + (4/3)\mu}{\rho}} \quad V_S = \sqrt{\frac{\mu}{\rho}}$$

where K is the bulk modulus, μ is the shear modulus, and ρ is the bulk density. The mass of each sample was recorded before the experiment, and the recorded changes in layer thickness were used to estimate changes in density by correcting for geometric thinning of the sample (e.g., [87]) and material losses.

To calculate effective porosity and density of our samples, we measured layer thickness under the applied load and used the known mass of each layer. Layer thickness was measured under load to a precision of $\pm 10\,\mu$m, and changes in thickness are known to $\pm 0.1\,\mu$m from digital measurements of the load point displacements (Fig. 1).

2.5 Experimental conditions

Experiments were run at room temperature and ambient humidity conditions. These parameters are recorded for each experiment and were relatively consistent over the suite of tests, but were not explicitly controlled. Previous work has established relationships between humidity and frictional strength for the materials used in our study [32,40,42]. Fluid saturation state has a significant effect on acoustic velocity and attenuation in geomaterials (e.g. [16,18,25,30,51,67,68,91]). However, our experiments were run under consistent, dry conditions [~10–20 % relative humidity] and thus sample to sample variations due to these effects are expected to be negligible (e.g. [99]).

3 Results

3.1 Effects of normal stress and compaction

We began each experiment by applying a small load normal to the sample (Fig. 4). Normal load was then increased in increments of 1 MPa, with waiting times of 10 s, during which we measured acoustic velocity. During periods of constant normal stress, samples undergo time-dependent, creep-compaction, consistent with previous observations (e.g., [32,47]). This compaction is responsible for part of the scatter seen in Fig. 4. We show both the range (lighter dots) and mean (larger, black symbols) of the ultrasonic velocities at each normal stress (Fig. 4). Ultrasonic velocity and density both increase with increasing normal stress (Fig. 4). Our data indicate that bulk density increases more slowly with increasing normal stress than elastic moduli, such that wave speed increases with increasing normal stress.

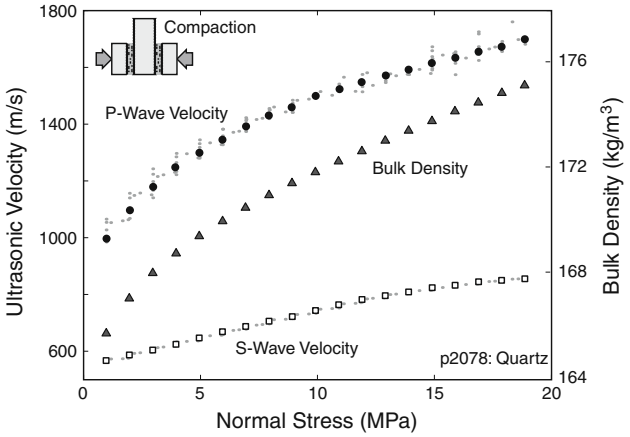

Fig. 4 The complete set of ultrasonic wave speed and density measurements for an experiment in which normal stress was applied in 1 MPa increments from 1 to 19 MPa. *Small grey points* indicate individual waveform picks, made as the sample was undergoing inelastic creep at constant stress, while *large points* represent average values at that normal stress

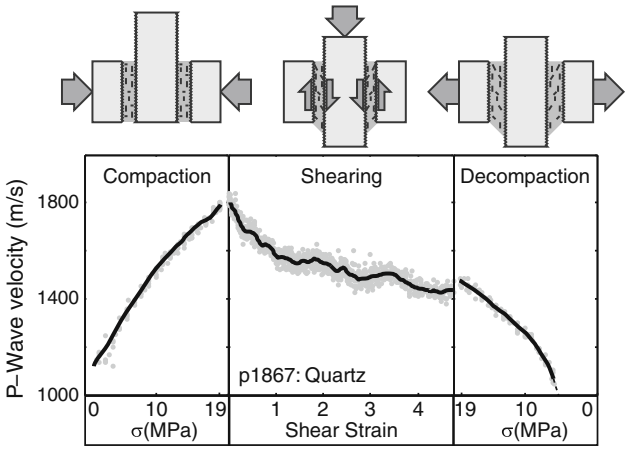

Fig. 5 Evolution of measured P-wave velocity during a full shear experiment, showing application of normal load, shear, and removal of normal load. *Grey points* indicate individual waveforms while the *solid line* indicates a moving-window average. Schematics above *each plot* indicate the relative movements of the forcing blocks and the sample during each stage. Velocity increases during application of normal load, due to porosity loss and densification, and decreases during shear due to grain fracture

3.2 Effects of shear strain

We explored the effect of two loading histories on sample behavior. One suite of experiments examined the effect of shear strain on wave velocity (Fig. 5). In these experiments, normal load was raised to 19 MPa and maintained at that level while samples were sheared at a continuous rate of 10 μm/s. The total shear displacement was approximately 22 millimeters, resulting in a shear strain of 4–5 (Fig. 5). The evolution of ultrasonic velocity and amplitude during each experiment may be divided into three stages (Fig. 5),

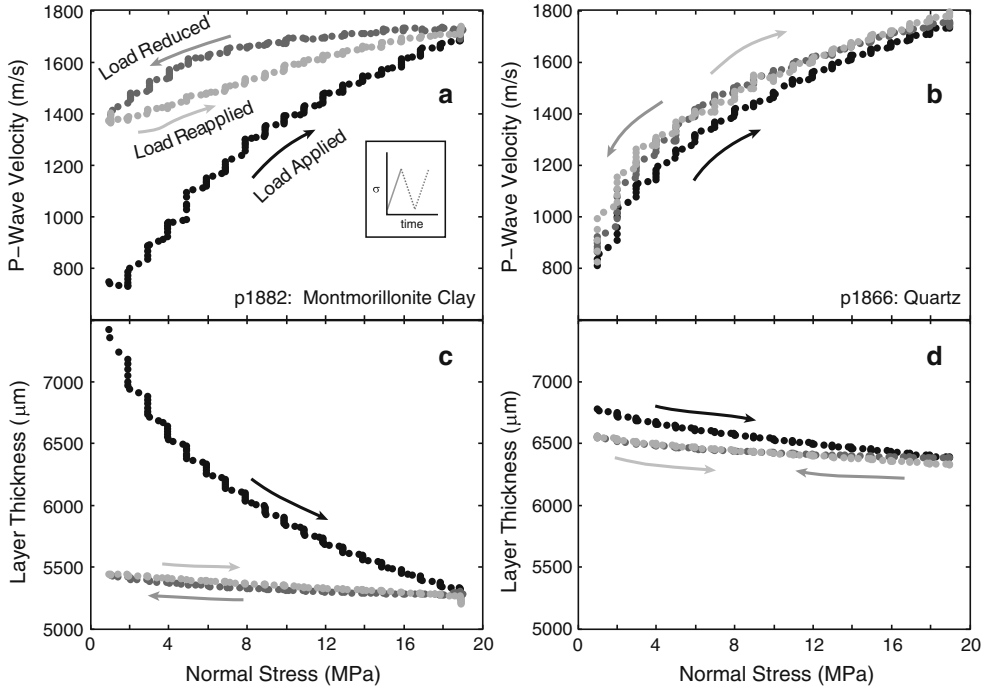

Fig. 6 Results for normal stress cycles on two sample types. Inset to panel **a** shows loading history. P-wave velocity increases (**a**, **b**) and the layer thins (**c**, **d**) as load is increased. Especially for the clay layer, when load is removed, the reduction in wave speed (**a**)—and the increase in layer thickness (**c**)—is small compared to the change upon initial loading. *Labels on arrows* in panel **a** apply to each panel. Note the effect of initial loading and hysteresis during subsequent loading and unloading

representing loading, shear strain accumulation, and unloading. We measure wave speed continuously during each stage. This suite of tests documents the relationship between sliding friction and elastic wave speed under fully mobilized, steady-state frictional sliding (Fig. 5).

The second suite of tests included experiments in which normal stress was cycled from 1 to 19 MPa and back in 1 MPa increments (Figs. 6, 7). These experiments investigated the effect of normal load on ultrasonic properties and also allowed assessment of the effect of macroscopic changes in granular packing and force chain geometry (e.g. [5,48,49,63]). Finally, the experiments with normal load cycles assessed hysteresis in stress–strain and acoustic properties as a function of strain. Figure 6 illustrates such tests for montmorillonite (6a, 6c) and quartz (6b, 6d).

P-wave velocity and relative amplitude evolve systematically as a function of normal load cycling. Figure 7 shows such data as a function of changes in layer thickness, expressed as linear strain normal to the layer. The darkest symbols indicate the initial, virgin, loading path, the intermediate color symbols show the effect of subsequent unloading to 1 MPa, and the lightest symbols indicate behavior for reloading to 19 MPa.

For each case, the virgin compaction curves differ from the subsequent unloading/reloading curves (Fig. 7). The clay layers exhibited the largest hysteresis loops, with large normal strain during virgin loading and large permanent strain upon unloading (Fig. 7). Permanent layer compaction is intermediate for the quartz-clay mixture, but the mixture shows significantly higher relative P-wave amplitude than either end-member.

For quartz and the quartz-clay mixture, P-wave velocity reduced to nearly its original value at the end of the virgin loading curve, whereas for the clay layer Vp was ~600 m/s higher than its initial value (Fig. 7) indicating permanent, inelastic deformation. As discussed below, this observation is important for understanding the ultrasonic data during coupled shear deformation and loading/unload cycles.

Load/unload cycles subsequent to the virgin loading curve are characterized by a quasi-linear relationship between Vp and P-wave amplitude as a function of normal strain, with only a small amount of inelastic strain (Fig. 7). The curves for ΔVp show a small concave-up section follow by a quasi-linear region until a yield point, after which wave speed rises more slowly and non-linearly with additional strain (Fig. 7). Relative amplitude also increased with loading and normal strain. Our data indicate that acoustic amplitude within the granular/clay mixtures increased with increasing contact stress and decreasing porosity along the path length between the source and receiver transducers (Figs. 6, 7). The values of Vp we measured are consistent with previous work [50,63,69,109,111].

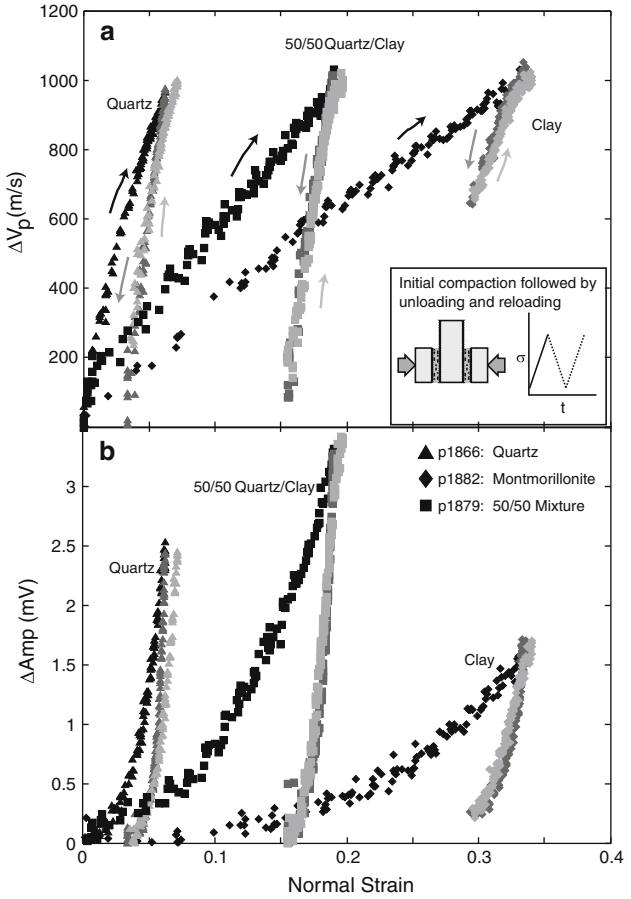

Fig. 7 Data from the same experiments shown in Fig. 6, with an additional experiment for a clay-quartz mixture. Inset to panel **a** shows loading history (see Fig. 6 for additional detail). *Each panel* shows changes in ultrasonic wave properties as a function of linear strain normal to the layer. **a** Change in P-wave velocity for a load-unload-reload cycle prior to shearing. **b** Change in relative P-wave amplitude. Note roughly linear relationship for velocity change with normal strain, after initial loading, and exponential increase in amplitude with compaction and strain

Shear strain has a significant effect on the properties of granular materials. We find that layer thickness, the coefficient of friction, P-wave velocity (Fig. 5), and P-wave amplitude all evolve systematically as a function of shear strain during loading and sliding (Fig. 8). Multiple experiments were run using each material, confirming that these trends are characteristic and reproducible. We explore the relationship between friction, wave velocity, and wave amplitude by comparing their variations with shear strain and normal stress. While we considered making direct plots of friction versus velocity, we found such plots difficult to interpret and instead, we rely on separate plots such as those shown in Figs. 8 and 9.

The granular layers thin along exponential decay curves (Fig. 8a), which represents the combined effects of shear-induced compaction, dilation, and geometric thinning due to shear [87]. The coefficient of friction for each material evolves non-linearly to a quasi steady-state value, which is generally reached by a shear strain of 2–3, consistent with previous work conducted at geophysical stresses (e.g., [65]).

Ultrasonic wave velocity and amplitude provide additional, independent information on how the materials evolve as a function of shear strain. The P-wave velocity of the quartz layers began to decrease immediately upon shearing, and continued to decrease as a function of shear strain, going from 1,750 to ∼1,500 m/s over a shear strain of 5 (Fig. 8c). P-wave amplitude for first arrivals through quartz layers decreased by 60–70 % at a shear strain of 0.5 and never recovered (Fig. 8d). In contrast, the clay layers exhibited an increase in P-wave velocity of about 100 m/s over a shear strain of 0.5 then decreased back to the initial value, and finally increased again for shear strains above about 2.5 (Fig. 8c). The behavior of the quartz-clay mixture was similar to that of the pure clay sample, with an initial increase in P-wave velocity of about 100 m/s followed by an equivalent decrease out to a shear strain of 1.5 and a gradual rise with increasing strain. As shear load increased, up to a shear strain of ∼1, the P-wave amplitude of the clay and the mixture decrease by ∼50 and 30 %, respectively, compared to the pre-shear values, but in both cases amplitude recovered with additional strain. It is interesting to note that P-wave velocity shows an initial peak, during the time when amplitude decreases, and then increases by a small amount with continued shear (Fig. 8). The initial peak in velocity for both materials coincided with a subtle decrease in the rate of layer thinning as a function of shear strain.

3.3 The effect of load cycles

We conducted a third suite of tests that included a combination of normal load cycles and increments of imposed shear strain (Fig. 9). In these experiments, normal stress was first stepped from 1 to 19 MPa in 1 MPa increments and then, with the normal stress at 19 MPa, we imposed a fixed shear displacement. These experiments provide data on the combined effects of changes in elastic properties, shear strain, and granular packing.

Shear strain and normal stress have a significant effect on ultrasonic wave speed in the quartz layers, a moderate effect in the mixture, and little change in the clay (Fig. 9a). P-wave velocity for the clay during these experiments tracked essentially the same curve as in the continuous shear experiments (e.g., compare to Fig. 8c), while the load cycles had little observable effect on either clay P-wave amplitude or long-term evolution of relative amplitude as a function of shear strain.

In contrast, for quartz and the mixture, the load-cycles had an immediate effect. Each time shearing resumed, the

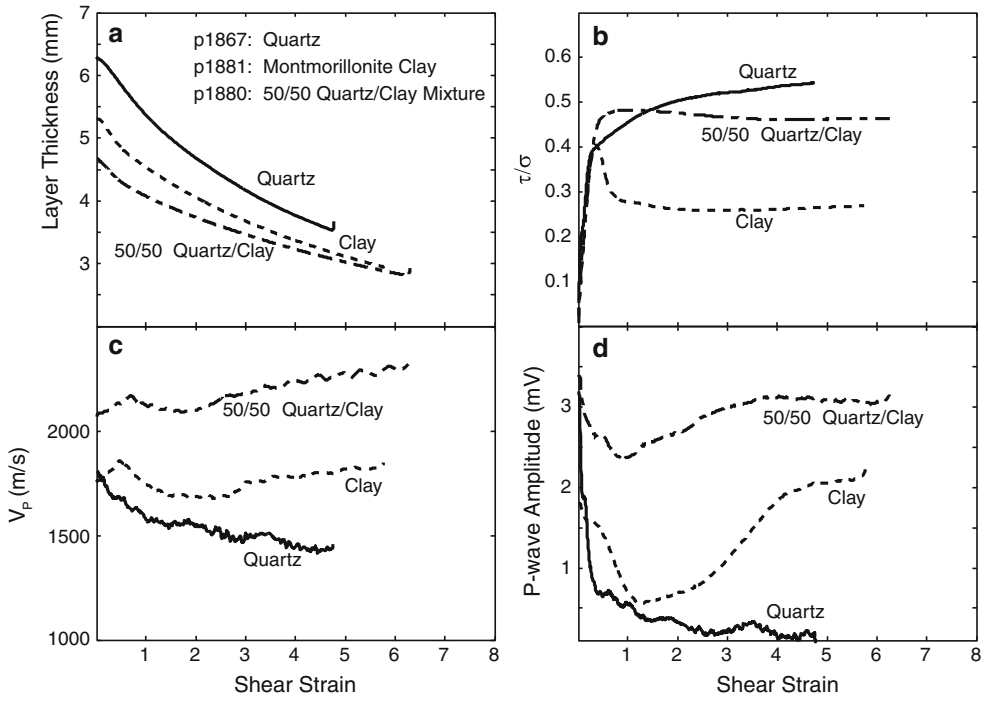

Fig. 8 Evolution of measured parameters as a function of shear strain. **a** Layer thickness, **b** coefficient of sliding friction, **c** P-wave velocity, and **d** relative P-wave amplitude. Note that amplitude decrease strongly as shear load is applied and then reaches a minimum and increases with further strain during steady-state frictional shear for the clay and clay-quartz mixture

P-wave velocity rose transiently, and then began to decrease over an increment of ~0.3–0.5 strain (Fig. 9a). This "bump" of 100–200 m/s in the record was observed following all five load-cycles. Moreover, rather than the overall decrease in P-wave velocity observed for the continuous shear experiments (Fig. 8c), the long-term average for the load-cycle experiments remained constant. The mixture displayed behavior similar to that of the quartz, although there was less of an observable direct effect following the resumption of shear deformation. Rather than the gradual increase in velocity observed during the continuous shear strain experiments, the P-wave velocity of the mixture during load-cycle experiments held close to a steady-state value with increasing strain (Fig. 9).

The coefficient of sliding friction for all three materials was largely unaffected by the normal stress cycles. There was an observable direct effect following the resumption of shear in the quartz samples, and a smaller effect in the mixture. In both cases the friction coefficient evolved toward values consistent with the continuous shear experiments illustrated in Fig. 8b. The effect on sample thickness was also subtle, but consistent with the idea that the granular framework of the quartz sample was changing more than that of the other materials. For the mixture and the pure clay, reducing the normal load caused the sample to expand, and reapplying the load caused it to contract by an equivalent amount. For the quartz, reducing the normal load did not induce a significant increase in layer thickness, but some thinning occurred when it was reapplied (Fig. 9c).

The evolution of relative wave amplitude during shear and normal load cycling was dramatic and similar for each sample (Fig. 9b). The P-wave amplitude of quartz layers increased by an amount ranging from 25 to 100 % of its previous value following each load cycle, then quickly decayed back to the original value of about 2 mV. The mixture displayed the same trend. Interestingly, the long-term increase in amplitude observed for the mixture in continuous sliding experiments (Fig. 8d) was replaced by an overall decrease. The amplitude of the clay samples exposed to periodic load cycles follows essentially the same trend as when sliding is continuous, with minimal perturbation associated with individual load cycles.

Figure 9a, b show velocity and amplitude versus shear strain. Because the shearing displacement is halted during a normal load cycle, changes in acoustic properties plot at a single strain value. The central, shaded, section in Fig. 9c shows detail of this behavior during a load cycle. Note that the velocity and amplitude decrease as a function of normal stress for the quartz, but when the normal stress is returned to 19 MPa both are at a much higher value than when shearing was halted.

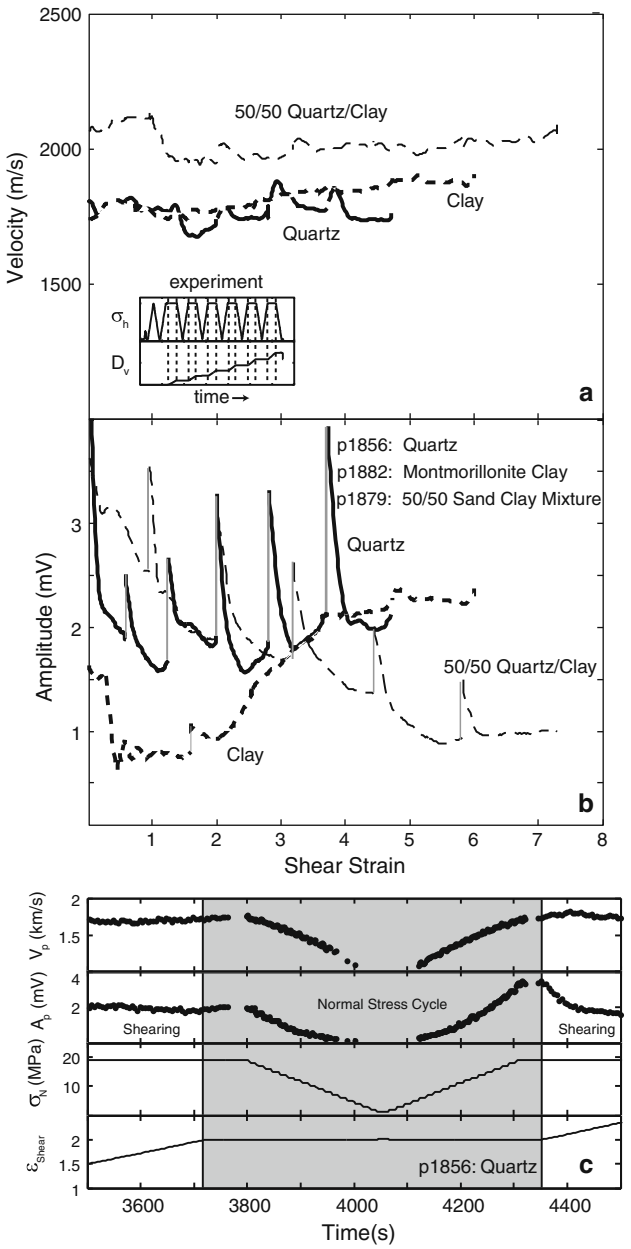

Fig. 9 Evolution of measured parameters as a function of shear strain during load-cycle experiments, including **a** P-wave velocity, and **b** relative P-wave amplitude. The *sharp vertical* discontinuities in both properties represent full load cycles in which both properties drop and recover. These points, as shown in one example load cycle **c** would collapse onto a single shear strain value and are therefore not evident in **a** and **b**

3.4 Elastic moduli

We combine the P and S-wave velocity with density measurements to determine the evolution of dynamic elastic moduli during our experiments (Fig. 10). Experiments with load cycles provide information on the elastic and inelastic properties and shear constitutive behavior during sample compaction (e.g., Fig. 6). Load-unload cycles during non-shearing portions of the experiment provide estimates of the quasi-static bulk modulus of each material. Our measurements show that these values vary with normal stress. The average values for our range of stresses are 0.64 GPa for quartz layers, 0.72 GPa for the mixture, and 0.61 GPa for clay. At a normal stress of 19 MPa, the dynamic moduli exhibit a greater spread, with values for quartz, the mixture, and clay of 3.5, 4.4 and 2.6 GPa, respectively. The dynamic shear moduli during compaction rose from 0.5 to 1.3 for quartz, 0.5 to 1.5 for the mixture and from 0.6 to 1.4 for clay (Fig. 10).

As the samples were sheared, the quartz and the mixture exhibited an initial drop in dynamic shear modulus (Fig. 10d, e). In the quartz sample the shear modulus reached a steady state at ∼1 GPa following this decrease. The shear modulus of the mixture recovered and continued to rise with increasing strain, ultimately reaching a value of ∼2 GPa by a strain of 5. The shear modulus of the clay layer rose by an amount similar to that of the clay-quartz mixture, which was significantly higher than observed for the pure, granular quartz (Fig. 10, compare panels d–f). The dynamic bulk modulus for all materials increased following the onset of shear, with the quartz reaching a value of ∼4 GPa, the clay beginning to come to steady state at 3.5 GPa and the mixture flattening off at around 8 GPa (Fig. 10).

4 Discussion

Granular materials accommodate shear strain and displacement through a variety of mechanisms. These include localization phenomena such as the formation of deformation bands (e.g. [23,46,79,80,93,94,105]) as well as network processes involving the creation and destruction of force chains (e.g. [8,41]). In dry or unsaturated granular samples deforming on a time scale of minutes to hours, we expect invariant physical and chemical properties of individual grains, although the average grain size and the shape of the size distribution may change with shear induced comminution. Furthermore, in an unsaturated sample the pores are filled with air at atmospheric pressure, which is likewise not expected to change appreciably during an experiment.

The evolution of ultrasonic velocity with normal stress and with shear strain (e.g. Fig. 5) must be attributable to changes in the granular contact stiffness, grain coordination number, porosity and load-supporting framework of the sample (e.g., [63]). A change in sample layer thickness implies a reorganization of grains, so the observed thinning corresponds to porosity reduction and an increasing granular coordination number. An increase in granular contact stiffness as well as in the granular coordination number will tend to increase wave velocity and amplitude [34]. In addition to the restructuring

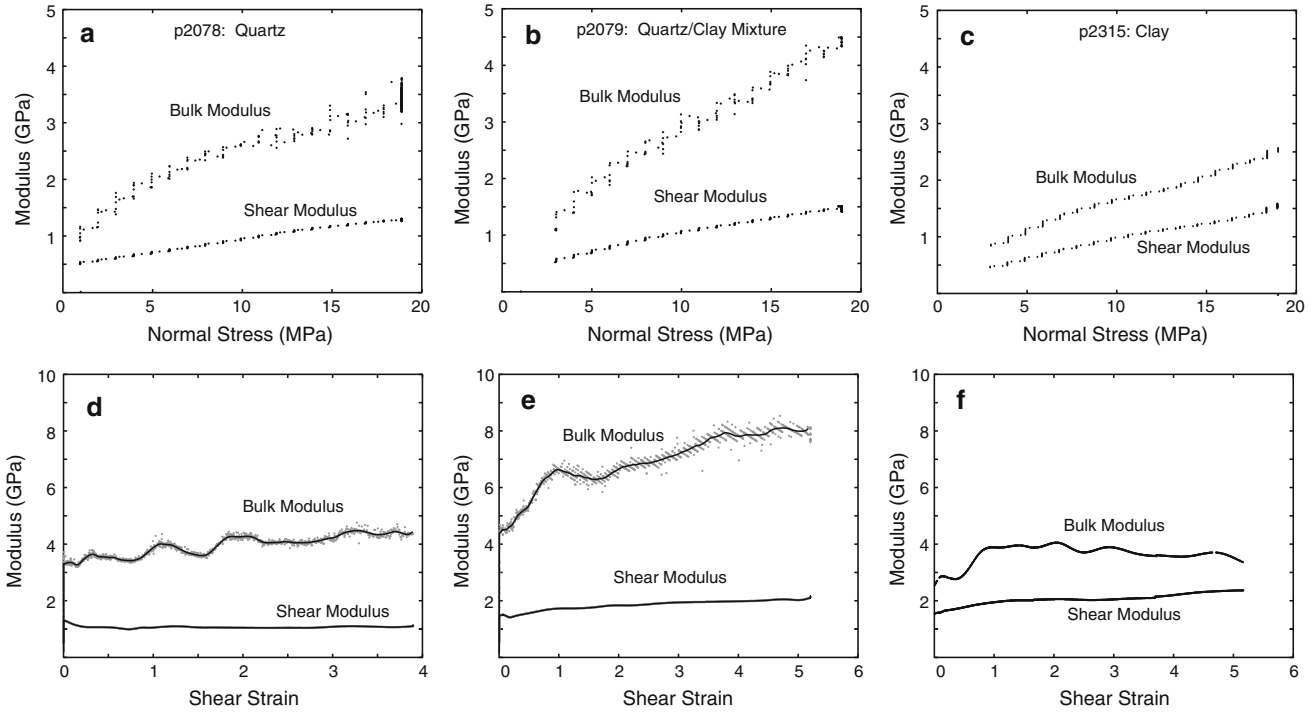

Fig. 10 Dynamic elastic moduli calculated from ultrasonic wave velocity and density. Moduli are plotted as a function of normal stress for **a** quartz, **b** a quartz/clay mixture, and **c** clay. Moduli are plotted as a function of shear strain for **d** quartz, **e** a quartz/clay mixture, and **f** clay

of grains into tighter arrangements, grain comminution will also decrease porosity.

Our measurements of ultrasonic properties indicate changes in elastic attenuation, as well as macroscopic measurements such as layer thickness (Fig. 8a) and frictional strength. Our friction curves (Fig. 8b) show an initial nonlinear increase as grains rearrange to accommodate shear displacement. The evolution of friction as a function of shear strain is characteristic of different materials sheared at different normal stresses, rates, and saturation states.

4.1 Stress distribution, granular processes and elastic properties

We find that wave velocity and amplitude of granular quartz decreases with shear (Fig. 8). This result was verified in multiple repeat experiments. At the pressures of our experiments one might expect wave velocity and amplitude to increase with shear strain, given that grains break with shear, which should broaden the particle size distribution and reduce porosity. However, granular contact stiffness and intragranular elastic properties of the granular framework also vary with shear strain. Indeed, the works of [48,49] show results similar to ours for shear of spherical beads, with reduction of P-wave speed upon shear.

Following [48,49], we hypothesize that wave velocity and amplitude of our sheared layers show the behavior indicated in Fig. 8 because of: (1) increase in intragranular crack density and the number of contact junctions, as comminution and spalling commence upon shearing, (2) rotation of the principal stress axis, which is initially normal to the layer and rotates through a minimum angle, at the peak of frictional stress, before reaching a steady value given by the granular friction angle, and (3) disruption of granular force chains. The amplitude of P-waves is affected most by principal stress orientation, as seen in the clay and quartz/clay mixtures (Fig. 8b, d). The clay layer shows the strongest peak stress and the biggest change in P-wave amplitude; however, the minimum in wave amplitude occurs after the peak stress, indicating that other factors are important.

During compaction and application of shear stress, force chains in the sample form to oppose the normal and shear stresses. For our sample configuration, the average orientation of these chains is expected to be subparallel to the direct path between the ultrasonic transducers. Given that the acoustic waveform is the sum of energy traveling through the network of force chains, and therefore will reflect changes in the mean orientation and stress state of grain-to-grain contacts, the observed reduction of wave speed with shear is consistent with destruction of longer trans-layer chains and formation of shorter chains and a more complex granular network (e.g., [24,49]).

The behavior of the quartz samples during the load-cycle experiments (Fig. 9) supports the idea that force chains are

important, as reducing the normal stress and reapplying it would reorder the force chains, as suggested in previous works (e.g., [47]). The long-term rotation of force chains through continuous shearing is disrupted, and neither amplitude nor velocity decays, in sharp contrast to the continuous shearing experiments (Fig. 8).

In contrast to granular layers, we do not expect that the clay layers will develop strong force chains that would reorient during load-cycles. Shear of clay samples occurs by localized slip along discrete surfaces in an R1 Riedel Shear orientation or along Y shears, rather than by the formation and destruction of distributed force chains. The lack of an effect on acoustic properties from load-unload cycles on the clay samples (Fig. 9) supports this interpretation.

The normal stress and shear stresses we apply at the boundaries of a sample will ultimately be resolved on many individual grain-to-grain contacts as "contact-normal" and "contact-tangent" stresses. The relationship between the boundary stresses and the population of contact stresses will be controlled by the arrangement of the granular framework. During initial loading of a granular material with no applied shear stress, we expect normal stress to be a more ideal proxy for isostatic pressure than during the shearing phase.

Ultrasonic velocity should vary systematically with properties of the granular layers. In particular, velocity should increase as contacts stiffen, porosity decreases, and grain coordination number increases, because waves will travel through more solid–solid interparticle contact junctions. This may explain the difference between the P-wave velocity curves for the quartz and the mixture (Fig. 7). The quartz sample starts out with higher wave speed, but is overtaken by the mixture as normal stress is increased. The curves for change in layer thickness for these materials (Fig. 6) indicate that the mixture compacts more than the pure quartz, which in turn indicates that the mixture experiences a larger reduction in porosity as a function of normal stress. This could explain why the effective bulk modulus of the mixture appears to increase more with strain than that of the pure quartz (Fig. 10), whereas the shear moduli of these materials do not differ significantly.

When we combine the behavior observed during compaction with that exhibited during shearing, we can explain the differences in effective moduli derived from wave speed. Our data suggest that differences in moduli are a product of differences in the evolution of packing for rounded to angular grains and platy clay particles as a function of shear strain accumulation (Fig. 11). The quartz grains compact into a tighter arrangement during loading (Fig. 11a). When sheared, the layers dilate as particles move over and around each other in order to accommodate strain (Fig. 11b). This produces a rotation of force chains away from the direct path between the transducers, as well as an increase in bulk porosity, both of which would cause a decrease in measured modulus and wave speed. Eventually the sample reaches a critical state (Fig. 11c) defined by a packing density that balances the load on the grains against the work required for dilation and shear. Concentrated loading of individual grains may cause communition through spalling or grain fracture [75], which would decrease bulk porosity but could increase crack porosity within grains, with a corresponding effect on ultrasonic velocity (e.g., [30]). The relative contribution of crack porosity has been demonstrated to dominate over the decrease in bulk porosity in cohesive sandstones undergoing cataclastic compaction [31].

Particle packing has an important effect on the ultrasonic properties of both clay and granular samples. The plate-like clay particles will be pushed into flatter orientations as the sample is compacted, but not completely (Fig. 11d). As the sample is sheared, some of these particles will be forced to kink and tear into configurations that permit sliding (Fig. 11e). This would result in a transient increase in strength as the sample dilates, causing an immediate decrease in wave amplitude as porosity increases but a wedge-shaped rise and fall in wave speed as observed in data presented in Fig. 8c, d. This may be an anisotropic effect caused by the average orientation of the particles rotating through the path between the transducers, which would result in an increase in apparent effective moduli when particles are more aligned with the wave propagation direction, even as the porosity is increasing. Alternatively, the fact that the clay sample has a higher coefficient of sliding friction during the dilatant phase (Fig. 8b) may mean that the average contact stresses are higher between grains or that additional force is expended in folding and kinking clay particles.

The p-wave speed, and elastic moduli, should increase with the maximum principal stress (e.g., [48]), and therefore an increase in shear stress, indicated by higher friction would, should result in an increase in wave speed. If porosity increases at the same time, amplitude should decrease. When a majority of clay grains lie in an orientation favorable to sliding, shear is expected to occur at constant volume or with slight compaction, resulting in a gradually increasing velocity and amplitude with shear (Fig. 11f).

The layers formed from the clay-quartz mixture have the widest particle size distribution, and therefore these should have the lowest porosity (Fig. 11g). Since the mixture behaves more like its clay end-member, we conclude that the clay "matrix" plays a more important role than the quartz grains in determining sample deformation and shear localization (Fig. 11h). Shear fabric in the mixtures seems to persist even during normal stress cycling (Fig. 11i).

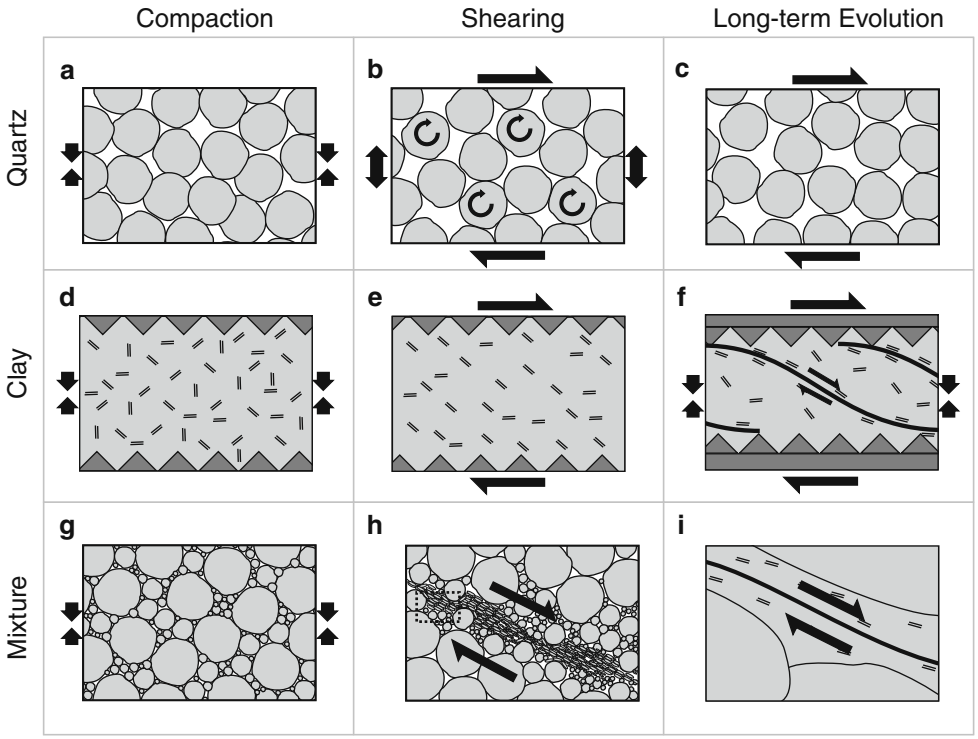

Fig. 11 Potential mechanisms responsible for differences in behavior observed for various materials during compaction, initial, and long-term shearing. For all materials, ultrasonic properties of the sheared layers are influenced by grain contact stiffness, coordination number, and grain size. Behavior of pure granular quartz layers is further influenced by dilation and force chain network. Clay layers are controlled by folding, kinking, and alignment. The mixture is controlled by localization of slip into clay-rich zones between quartz grains

4.2 Microstructural observations

We tested the mechanical hypotheses developed from our constitutive data by examining the samples post-shear using a Scanning Electron Microscope. The samples are initially unconsolidated (Fig. 2), but after compaction and shearing, they gain cohesion. For the layers of clay and quartz-clay, post-shear cohesion is sufficient that they can be removed from the experimental apparatus as solid pieces that separate along shear fabric surfaces [36,65]. The low permeability and cohesion of these samples makes them difficult to impregnate with epoxy and polish for thin sections, but we were able to image surfaces of shear fabric (localization features) and the edges of fracture pieces. We fractured samples parallel to the shear direction to view the cross-sectional distribution of shear structures (Fig. 12). The layers of pure quartz did not retain sufficient cohesion following shear to permit similar analysis.

What we find is that the failure surfaces present in the clay layers and in the mixture are extremely similar, with clay-rich failure planes localizing deformation between the quartz grains found in the mixture. Clay content is important in determining the behavior of fault gouge, and a great deal of work has been done to understand the transition from a clast-supported system to a matrix-supported system (e.g. [36,42,43]). The strain localization we observe at 50 % clay content is similar to that which occurred in pure clay experiments, but in the mixture these localization planes form in regions of continuous clay matrix and between masses of larger clasts (Fig. 12).

Given the higher P-wave velocity observed in the mixture, but the similarity in trends observed in the mixture and the clay layer during shearing (Fig. 8), we infer that the zero-order dynamic elastic properties of the sample are controlled mainly by differences in porosity rather than the relative percentages of quartz and clay. However, the evolution with shear strain is dominated by the formation of clay localization surfaces rather than the formation of force chains between larger grains. This behavior is more obvious in the ultrasonic velocity data than in measurements of the bulk coefficient of sliding friction. The relative weakness of the clay samples compared with the mixture may simply be due to the fact that deformation in a shearing clay layer can be distributed over more surfaces (Fig. 12e). Further experiments are needed to identify how velocity varies as a function of shear strain as a critical percentage of quartz grains is reached such that shear transitions from a matrix localization process to grain-supported force chains.

5 Conclusions

We instrumented a biaxial double direct shear configuration to make precise measurements of ultrasonic P and S-wave velocity during shear of granular and clay materi-

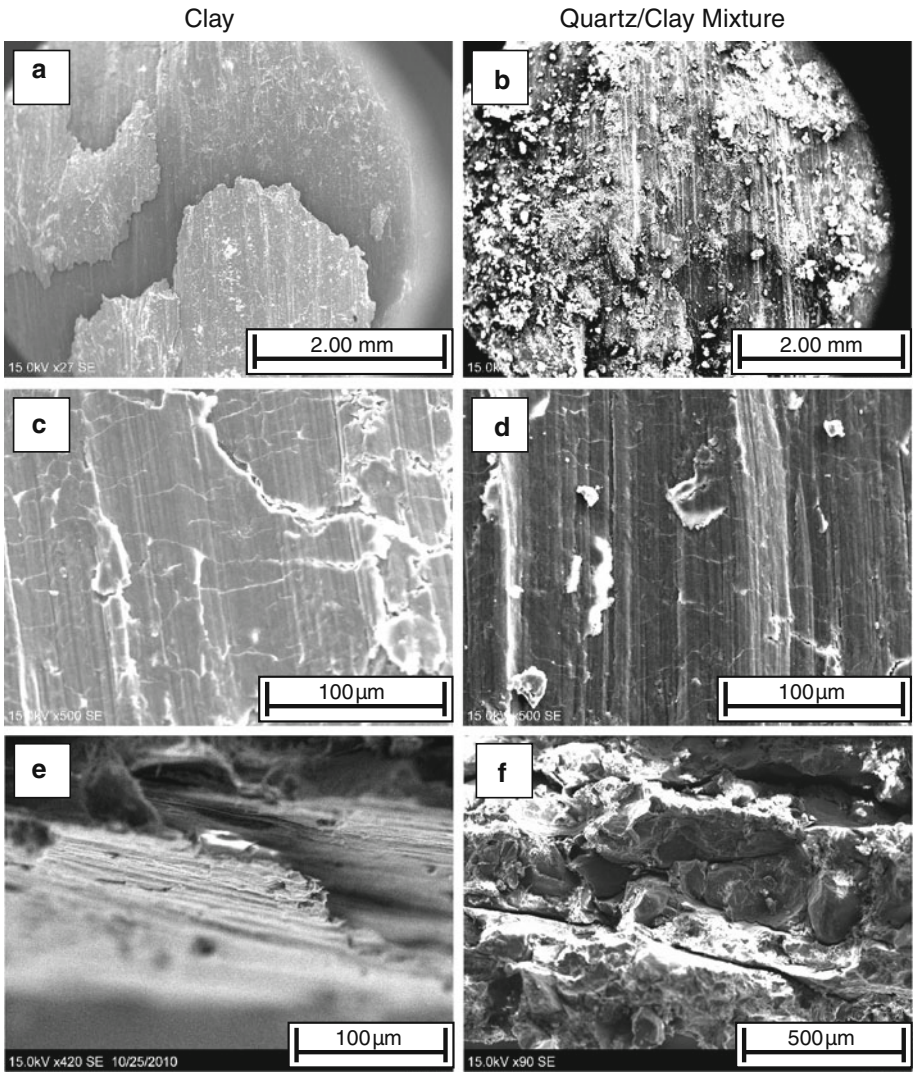

Fig. 12 Scanning Electron Microscope images of clay and quartz/clay mixture samples following shearing. **a**, **b** show shear fabric surfaces with slickenlines formed in both clay and the mixture, respectively. **d**, **e** show a closer view of these surfaces, drawing attention to the similarity in the spacing of grooves and the absence of larger grains along the surfaces. **e**, **f** show similar surfaces in cross-section, emphasizing the tight spacing of parallel slip surfaces in the clay sample **e** compared with the thick zones of mixed quartz and clay

als subjected to elevated normal stress. Our system allows for high-resolution measurement of changes in travel time and wave amplitude as a function of shear and other factors in a given experiment. Measurements of wave speed during compaction are in good agreement with values from prior research. Measurements are repeatable and characteristic differences are present between the range of granular materials tested. The evolution of effective elastic moduli as calculated by changes in velocity and density (porosity) during shear helps to constrain the micromechanics of shearing of granular materials. The continual decrease of wave speed and effective moduli in quartz layers suggests sample dilation and porosity increase during formation and evolution of force chains across the shearing layer, whereas the complex evolution of velocity and amplitude in the clay and clay/quartz mixture suggest initial dilation upon shearing followed by porosity reduction and localization with increasing shear strain. Light microscopy and SEM images demonstrates that shear localization occurs in both clay samples and the quartz/clay mixtures. These observations and techniques can be extended to a range of natural materials, including gouge from tectonic fault zones.

Acknowledgments We thank C. Carpenter, B. Kaproth and S. Swavely for assistance in the lab, and S. Haines for help with SEM work. We thank two anonymous reviewers for comments that improved the paper greatly. This work was supported by NSF grants OCE-0648331, EAR-0746192, and EAR-0950517.

References

1. AnhDan, L., Koseki, J., Sato, T.: Comparison of Young's moduli of dense sand and gravel measured by dynamic and static methods. Geotech. Test. J. **25**(4) (2002). doi:10.1520/GTJ11290J
2. Anthony, J., Marone, C.: Influence of particle characteristics on granular friction. J. Geophys. Res. **110** (2005). doi:10.1029/2004JB003399
3. Bachrach, R., Avseth, P.: Rock physics modeling of unconsolidated sands: accounting for nonuniform contacts and heterogeneous stress fields in the effective media approximation with appli-

cations to hydrocarbon exploration. Geophysics **73**(6) (2008). doi:10.1190/1.2985821
4. Bachrach, R., Dvorkin, J., Nur, A.M.: Seismic velocities and Poisson's ratio of shallow unconsolidated sands. Geophysics **65**(2) (2000). doi:10.1190/1.1444751
5. Behringer, R.P., Daniels, K.E., Majmudar, T.S., Sperl, M.: Fluctuations, correlations and transitions in granular materials: statistical mechanics for a non-conventional system. Philos. Trans. R. Soc. A **366** (2008). doi:10.1098/rsta.2007.2106
6. Berryman, J.G.: Long-wavelength propagation in composite elastic media II. Ellipsoidal inclusions. J. Acoust. Soc. Am. **68**, 1820–1831 (1980)
7. Berryman, J.G., Pride, S.R., Wang, H.F.: A differential scheme for elastic properties of rocks with dry or saturated cracks. Geophys. J. Int. **151**, 597–611 (2002)
8. Bocquet, L., Losert, W., Schalk, D., Lubensky, T.C., Gollub, J.P.: Granular shear flow dynamics and forces: experiment and continuum theory. Phys. Rev. E **65** (2001). doi:10.1103/PhysRevE.65.011307
9. Boitnott, G.N., Biegel, R.L., Scholz, C.H., Yosioka, N., Wang, W.: Micromechanics of rock friction, 2: quantitative modeling of initial friction with contact theory. J. Geophys. Res. **97**, 8965–8978 (1992)
10. Boudjema, M., Santos, I.B., McCall, K.R., Guyer, R.A., Boitnott, G.N.: Linear and nonlinear modulus surfaces in stress space, from stress-strain measurements on Berea sandstone. Nonlinear Proc. Geophys. **10**, 589–597 (2003)
11. Bourbié, T., Coussy, O., Zinszner, B.: Acoustics of Porous Media. Gulf Pub. Co, Editions Technip) (1987)
12. Bradbury, K.K., Barton, D.C., Solum, J.G., Draper, S.D., Evans, J.P.: Mineralogic and textural analyses of drill cuttings from the San Andreas fault observatory at depth (SAFOD) boreholes: initial interpretations of fault zone composition and constraints on geologic models. Geosphere **3** (2007). doi:10.1130/GES00076.1
13. Blum, T.E., Snieder, R., van Wijk, K., Willis, M.E.: Theory and laboratory experiments of elastic wave scattering by dry planar fractures. J. Geophys. Res. **116**, B08218 (2011). doi:10.1029/2011JB008295
14. Brignoli, E.G.M., Gotti, M., Stokoe, II, K.H.: Measurement of shear waves in laboratory specimens by means of piezoelectric transducers. ATSM Geotech. Test. J. **19**(4) (1996). doi:10.1520/GTJ10716J
15. Brunet, T., Jia, X., Johnson, P.A.: Transitional nonlinear elastic behaviour in dense granular media. Geophys. Res. Lett. **35**, L19308 (2008). doi:10.1029/2008GL035264
16. Buckingham, M.J.: Theory of acoustic attenuation, dispersion, and pulse propagation in unconsolidated granular materials including marine sediments. J. Acoust. Soc. Am. **102**(5) (1997). doi:10.1121/1.420313
17. Byerlee, J.: Friction of rocks. Pure Appl. Geophys. **116**(4–5) (1978). doi:10.1007/BF00876528
18. Cadoret, T., Marion, D., Zinszner, B.: Influence of frequency and fluid distribution on elastic wave velocities in partially saturated limestones. J. Geophys. Res. **100**(B6) (1995). doi:10.1029/95JB00757
19. Carpenter, B.M., Marone, C., Saffer, D.M.: Frictional strength of the san andreas fault from laboratory measurements of SAFOD drill samples. Nat. Geosci. (2011). doi:10.1038/ngeo1089
20. Carpenter, B.M., Saffer, D.M., Marone, C.: Frictional properties and sliding stability of the San Andreas fault from deep drill core. Geology **40**, 759–762 (2012). doi:10.1130/G33007
21. Cascante, G., Santamarina, J.C.: Interparticle contact behavior and wave propagation. J. Geotech. Geoenviron. Eng. **122**, 831–839 (1996)
22. Chester, F.M., Evans, J.P., Biegel, R.K.: Internal structure and weakening mechanisms of the San Andreas fault. J. Geophys. Res. **98**(B1) (1993). doi:10.1029/92JB01866
23. Chupin, O., Rechenmacher, A.L., Abedi, S.: Finite strain analysis of non-uniform deformations in shear bands in Sand. Int. J. Numer. Anal. Methods Geomech. **36**, 1651–1666 (2010). doi:10.1002/nag.1071
24. Daniels, K.E., Hayman, N.W.: Force chains in seismogenic faults visualized with photoelastic granular shear experiments. J. Geophys. Res. **113**, B11411 (2008). doi:10.1029/2008JB005781
25. David, E.C., Zimmerman, R.W.: Pore structure model for elastic wave velocities in fluid-saturated sandstones. J. Geophys. Res. **117**, B07210 (2012). doi:10.1029/2012JB009195
26. Dieterich, J.H.: Modeling of rock friction 1. Experimental results and constitutive equations. J. Geophys. Res. **84**(B5) (1979). doi:10.1029/JB084iB05p02161
27. Dieterich, J.H.: Constitutive properties of faults with simulated gouge. In: Carter, N.L., Friedman, M., Logan, J.M., Stearns, D.W. (eds.) Mechanical Behavior of Crustal Rocks. AGU Monograph, vol. 24, pp. 103–120. Washington DC, AGU (1981)
28. Dvorkin, J., Nur, A.: Dynamic poroelasticity: a unified model with the squirt and the Biot mechanisms. Geophysics **58**(4) (1993). doi:10.1190/1.1443435
29. Estep, J., Dufek, J.: Substrate effects from force chain dynamics in dense granular flows. J. Geophys. Res. **117**, F01028 (2012). doi:10.1029/2011JF002125
30. Fortin, J., Schubnel, A., Guéguen, Y.: Elastic wave velocities and permeability evolution during compaction of Bleurswiller sandstone. Int. J. Rock Mech. Min. **42** (2005). doi:10.1016/j.ijrmms.2005.05.002
31. Fortin, J., Guéguen, Y., Schubnel, A.: Effects of pore collapse and grain crushing on ultrasonic velocities and V_p/V_s. J. Geophys. Res. **112**(B0827) (2007). doi:10.1029/2005JB004005
32. Frye, K.M., Marone, C.: Effect of humidity on granular friction at room temperature. J. Geophys. Res. **107**(B11) (2002). doi:10.1029/2001JB000654
33. Gassmann, F.: Elastic waves through a packing of spheres. Geophysics **16** (1951). doi:10.1190/1.1437718
34. Goddard, J.D.: Nonlinear elasticity and pressure-dependent wave speeds in granular media. Proc. R. Soc. Lond. A Mat. **430**(1878) (1990). doi:10.1098/rspa.1990.0083
35. Goren, L., Aharonov, E., Sparks, D., Toussaint, R.: The mechanical coupling of fluid-filled granular material under shear. Pure Appl. Geophys. **168**, 2289–2323 (2011). doi:10.1007/s00024-011-0320-4
36. Haines, S.H., van der Pluijm, B.A., Ikari, M., Saffer, D., Marone, C.: Clay fabrics in natural and artificial fault gouge. J. Geophys. Res. **114**(B5), B05406 (2009). doi:10.1029/2008JB005866
37. Han, D., Batzle, M.: Velocities of deepwater reservoir sands. Leading Edge **25** (2006). doi:10.1190/1.2193222
38. Hertz, H.: Über die Berührung fester elasticher Körper. Journal für die reine und angewandte Mathematik **92**, 156–171 (1881)
39. Hobiger, M., Wegler, U., Shiomi, K., Nakahara, H.: Coseismic and postseismic elastic wave velocity variations caused by the 2008 Iwate-Miyagi Nairiku earthquake. Jpn. J. Geophys. Res. **117**, B09313 (2012). doi:10.1029/2012JB009402
40. Hong, T., Marone, C.: Effects of normal stress perturbations on the frictional properties of simulated faults. Geochem. Geophys. Geosyst. **6**(3) (2005). doi:10.1029/2004GC000821
41. Howell, D.W., Behringer, R.P., Veje, C.T.: Fluctuations in granular media. Chaos **9**(3) (1999). doi:10.1063/1.166430
42. Ikari, M.J., Saffer, D.M., Marone, C.: Effect of hydration state on the frictional properties of montmorillonite-based fault gouge. J. Geophys. Res. **112**(B06423) (2007). doi:10.1029/2006JB004748

43. Ikari, M., Saffer, D.M., Marone, C.: Frictional and hydrologic properties of clay-rich fault gouge. J. Geophys. Res. **114**, B05409 (2009). doi:10.1029/2008JB006089
44. Jia, X.: Ultrasound propagation in disordered granular media. Mat. Res. Soc. Symp. Proc. 627 (2000).
45. Jia, X., Caroli, C., Velicky, B.: Ultrasound propagation in externally stressed granular media. Phys. Rev. Lett. **82**(9) (1999). doi:10.1103/PhysRevLett.82.1863
46. Kaproth, B.M., Cashman, S.M., Marone, C.: Deformation band formation and strength evolution in unlithified sand: the role of grain breakage. J. Geophys. Res. **115**, B12103 (2010). doi:10.1029/2010JB007406
47. Karner, S.L., Marone, C.: Frictional restrengthening in simulated fault gouge: effect of shear load perturbations. J. Geophys. Res. **106**, 19319–19337 (2001)
48. Khidas, Y., Jia, X.: Anisotropic nonlinear elasticity in a spherical-bead pack: influence of the fabric anisotropy. Phys. Rev. E **81**, 021303 (2010)
49. Khidas, Y., Jia, X.: Probing the shear-band formation in granular media with sound waves. Phys. Rev. E **85**, 051302 (2012)
50. King, M.S.: Wave velocities in rocks as a function of changes in overburden pressure and pore fluid saturants. Geophysics **31**(1) (1966). doi:10.1190/1.1439763
51. Knight, R., Dvorkin, J., Nur, A.: Acoustic signatures of partial saturation. Geophysics **63**(1) (1998). doi:10.1190/1.1444305
52. Knopoff, L.: Q. Rev. Geophys. **2**(4), 625–660 (1964). doi:10.1029/RG002i004p00625
53. Knuth, M., Marone, C.: Friction of sheared granular layers: the role of particle dimensionality, surface roughness, and material properties. Geochem. Geophys. Geosyst. **8**, Q03012 (2007). doi:10.1029/2006GC001327
54. Lay, T., Ammon, C.J., Hutko, A.R., Kanamori, H.: Effects of kinematic constraints on teleseismic finite-source rupture inversions: Great Peruvian Earthquakes of 23 June 2001 and 15 August 2007. Bull. Seismol. Soc. Am. **100**(3) (2010). doi:10.1785/0120090274
55. Lee, J.Y., Francisca, F.M., Santamarina, J.C., Ruppel, C.: Parametric study of the physical properties of hydrate-bearing sand, silt, and clay sediments: 2. Small-strain mechanical properties. J. Geophys. Res. **115**, B11105 (2010). doi:10.1029/2009JB006670
56. Linker, M.F., Dieterich, J.H.: Effects of variable normal stress on rock friction: observations and constitutive equations. J. Geophys. Res. **97**(B4) (1992). doi:10.1029/92JB00017
57. Liu, C.-h., Nagel, S.R.: Sound in sand. Phys. Rev. Lett. **68**(15) (1992). doi:10.1103/PhysRevLett.68.2301
58. Maeda, N.: A method for reading and checking phase times in autoprocessing system of seismic wave data. Jishin (J. Seismol. Soc. Jpn.) **38**, 365–379 (1985)
59. Mainprice, D., Page, Y.L., Rodgers, J., Jouanna, P.: Ab initio elastic properties of talc from 0 to 12 GPa: interpretation of seismic velocities at mantle pressures and prediction of auxetic behaviour at low pressure. Earth Planet Sci. Lett. **274** (2008). doi:10.1016/j.epsl.2008.07.047
60. Mair, K., Marone, C.: Friction of simulated fault gouge for a wide range of velocities and normal stresses. J. Geophys. Res. **104**, 28899–28914 (1999)
61. Mair, K., Frye, K.M., Marone, C.: Influence of grain characteristics on the friction of granular fault zones. J. Geophys. Res. **107**(B10):2219 (2002)
62. Majmudar, T.S., Behringer, R.P.: Contact force measurements and stress-induced anisotropy in granular materials. Nature **435** (2005). doi:10.1038/nature03805
63. Makse, H.A., Gland, N., Johnson, D.L., Schwartz, L.: Granular packings: nonlinear elasticity, sound propagation, and collective relaxation dynamics. Phys. Rev. E **70**(6), 061302 (2004). doi:10.1103/PhysRevE.70.061302
64. Manjunath, M., Awasthi, A.P., Geubelle, P.H.: Wave propagation in random granular chains. Phys. Rev. E **85**, 031308 (2012)
65. Marone, C.: Laboratory-derived friction laws and their application to seismic faulting. Annu. Rev. Earth Planet Sci. **26**, 643–696 (1998). doi:10.1146/annurev.earth.26.1.643
66. Marone, C., Carpenter, B.M., Schiffer, P.: Transition from rolling to jamming in thin granular layers. Phys. Rev. Lett. **101**, 248001 (2008). doi:10.1103/PhysRevLett.101.248001
67. Mavko, G.: Velocity and attenuation in partially molten rocks. J. Geophys. Res. **85**, 5173–5189 (1980)
68. Mavko, G., Nur, A.: Wave attenuation in partially saturated rocks. Geophysics **44**, 161–178 (1979)
69. Mavko, G., Mukerji, T., Dvorkin, J.: The Rock Physics Handbook. Cambridge University Press, New York (1998)
70. Mindlin, R.D.: Mechanics of Granular Media. Columbia University Press, New York (1954)
71. Molyneux, J.B., Schmitt, D.R.: First-break timing: Arrival onset times by direct correlation. Geophysics **64**(5) (1999). doi:10.1190/1.1444653
72. Mühlhaus, H., Oka, F.: Dispersion and wave propagation in discrete and continuous models for granular materials. Int. J. Solids Struct. **33**, 2841–2858 (1996). doi:10.1016/0020-7683(95)00178-6
73. Papargyri-Beskou, S., Mylonakis, G.: Wave dispersion studies in granular media by analytical and analytical-numerical methods. Soil Dyn. Earthq. Eng. **29** (2009). doi:10.1016/j.soildyn.2008.10.003
74. Peraldi, R., Clement, A.: Digital processing of refraction data study of first arrivals. Geophys. Prospect. **20**(3) (2006). doi:10.1111/j.1365-2478.1972.TB00653
75. Pittman, E.: Effect of fault-related granulation on porosity and permeability of quartzstones, Simpson Group (Ordovician) Oklahoma. Am. Assoc. Pet. Geol. Bull. **65**(11), 2381–2387 (1981)
76. Prasad, M., Meissner, R.: Attenuation mechanisms in sands: laboratory versus theoretical (Biot) data. Geophysics **57**(5) (1992). doi:10.1190/1.1443284
77. Radjai, F., Wolf, D.E., Jean, M., Moreau, J.-J.: Bimodal character of stress transmission in granular packings. Phys. Rev. Lett. **80**(1) (1998). doi:10.1103/PhysRevLett.80.61
78. Rathbun, A.P., Marone, C.: Effect of strain localization on frictional behavior of sheared granular materials. J. Geophys. Res. **115**, B01204 (2010). doi:10.1029/2009JB006466
79. Rawling, G.C., Goodwin, L.B.: Cataclasis and particulate flow in faulted, poorly lithified sediments. J. Struct. Geol. **25** (2003). doi:10.1016/S0191-8141(02)00041-X
80. Rechenmacher, A.L.: Grain-scale processes governing shear band initiation and evolution in sands. J. Mech. Phys. Solids **54**, 22–45 (2006)
81. Rechenmacher, A., Abedi, S., Chupin, O.: Evolution of force chains in shear bands in sand. Geotechnique **60**, 343–351 (2010)
82. Rose, J.L.: Ultrasonic Waves in Solid Media. Cambridge University Press, New York (1999)
83. Santamarina, J.C., Cascante, G.: Stress anisotropy and wave propagation: a micromechanical view. Can. Geotech. J. **33**, 770–782 (1996)
84. Savage, J.C.: Attenuation of elastic waves in granular mediums. J. Geophys. Res. **70**, 3935–3942 (1965)
85. Schenker, I., Filser, F.T., Hütter, M., Gauckler, L.J.: The influence of the degree of heterogeneity on the elastic properties of random sphere packings. Granul. Matter **14**, 333–340 (2012). doi:10.1007/s10035-012-0316-5
86. Scholz, C.H.: Earthquakes and friction laws. Nature **391** (1998). doi:10.1038/34097
87. Scott, D.R., Marone, C., Sammis, C.G.: The apparent friction of granular fault gouge in sheared layers. J. Geophys. Res. **99**(B4) (1994). doi:10.1029/93JB03361

88. Segall, P., Rice, J.R.: Dilatancy, compaction, and slip instability of a fluid-infiltrated fault. J. Geophys. Res. **100**(B11) (1995). doi:10.1029/95JB02403
89. Sibson, R.H.: Fault rocks and fault mechanics. J. Geol. Soc. Lond. **133** (1997). doi:10.1144/gsjgs.133.3.0191
90. Sleep, N.H.: Microscopic elasticity and rate and state friction evolution laws. Geochem. Geophys. Geosyst. **13**, Q12002 (2012). doi:10.1029/2012GC004393
91. Stoll, R.D.: Velocity dispersion in water-saturated granular sediment. J. Acoust. Soc. Am. **111**(2) (2002). doi:10.1121/1.1432981
92. Terzaghi, K.: The shearing resistance of saturate soils. In: Proceedings of the 1st International Conference on Soil Mechanism, vol. 1, pp. 54–56 (1936)
93. Tordesillas, A.: Force chain buckling, unjamming transitions and shear banding in dense granular assemblies. Philos. Mag. **87**(32) (2007). doi:10.1080/14786430701594848
94. Tordesillas, A., Muthuswamy, M.: On the modeling of confined buckling of force chains. J. Mech. Phys. Solids **57** (2009). doi:10.1016/j.jmps.2009.01.005
95. van der Elst, N.J., Brodsky, E.E., Le Bas, P.-Y., Johnson, P.A.: Auto-acoustic compaction in steady shear flows: experimental evidence for suppression of shear dilatancy by internal acoustic vibration. J. Geophys. Res. **117**, B09314 (2012). doi:10.1029/2011JB008897
96. Vermilye, J.M., Scholz, C.H.: The process zone: a microstructural view of fault growth. J. Geophys. Res. **103**(B6) (1998). doi:10.1029/98JB00957
97. Vernik, L., Nur, A.: Ultrasonic velocity and anisotropy of hydrocarbon source rocks. Geophysics **57**(5) (1992). doi:10.1190/1.1443286
98. Vilchinska, N.A.: Force chains in granular media and ultrasound impulse propagation in sand specimen under load. Tech. Acoust. **20**, 213–217 (2007)
99. Vlahinić, I., Jennings, H.M., Thomas, J.J.: A constitutive model for drying of a partially saturated porous material. Mech. Mater. **41** (2009). doi:10.1016/j.mechmat.2008.10.011
100. Voltolini, M., Wenk, H.-R., Mondol, M.H., Bjørlykke, K., Jahren, J.: Anisotropy of experimentally compressed kaolinite-illite-quartz mixtures. Geophysics **74**(1) (2009). doi:10.1190/1.3002557
101. Wang, H.: Quasi-static poroelastic parameters in rock and their geophysical applications. Pure Appl. Geophys. **141** (1993). doi:10.1007/BF00998332
102. Wang, Y.-H., Santamarina, J.C.: Attenuation in sand: an exploratory study on the small-strain behavior and the influence of moisture condensation. Granul. Matter **9**(6), 365–376 (2007)
103. Winkler, K., Nur, A., Gladwin, M.: Friction and seismic attenuation in rocks. Nature **227**, 528–531 (1979)
104. Winkler, K.W., Nur, A.: Seismic attenuation: effects of pore fluids and frictional sliding. Geophysics **47**, 1–15 (1982)
105. Wolf, H., König, D., Triantafyllidis, T.: Experimental investigation of shear band patterns in granular material. J. Struct. Geol. **25** (2003). doi:10.1016/S0191-8141(02)00163-3
106. Zhang, H., Thurber, C., Rowe, C.: Automatic *P*-wave arrival detection and picking with multiscale wavelet analysis for single-component recordings. Bull. Seismol. Soc. Am. **93**(5) (2003). doi:10.1785/0120020241
107. Zheng, B., Elsworth, D.: Evolution of permeability in heterogeneous granular aggregates during chemical compaction: ranular mechanics models. J. Geophys. Res. **117**, B03206 (2012). doi:10.1029/2011JB008573
108. Zienkiewicz, O.C., Chan, A.H.C., Pastor, M., Paul, D.K., Shiomi, T.: Static and dynamic behavior of soils: a rational approach to quantitative solutions. I. Fully saturated problems. Proc. R. Soc. Lond. A Mat. **429**(1877) (1990). doi:10.1098/rspa.1990.0061
109. Zimmer, M.A.: Seismic velocities in unconsolidated sands: measurements of pressure, sorting, and compaction effects. Ph.D. dissertation, Stanford University (2003)
110. Zimmer, M., Prasad, M., Mavko, G.: Pressure and porosity influences on $V_P - V_S$ ratio in unconsolidated sands. Leading Edge **21**(2) (2002). doi:10.1190/1.1452609
111. Zimmer, M.A., Prasad, M., Mavko, G., Nur, A.: Seismic velocities of unconsolidated sands: part 1—pressure trends from 0.1 to 20 MPa **72**(1) (2007a). doi:10.1190/1.2399459
112. Zimmer, M.A., Prasad, M., Mavko, G., Nur, A.: Seismic velocities of unconsolidated sands: part 2—influence of sorting- and compaction-induced porosity variation. Geophysics **72**(1) (2007). doi:10.1190/1.2364849